Oncogene (2021) 40:1300–1317
https://doi.org/10.1038/s41388-020-01604-5

ARTICLE

A feed-forward loop between SorLA and HER3 determines heregulin response and neratinib resistance

Hussein Al-Akhrass[1] · James R. W. Conway[1] · Annemarie Svane Aavild Poulsen[2] · Ilkka Paatero[1] · Jasmin Kaivola[1] · Artur Padzik[1] · Olav M. Andersen[2] · Johanna Ivaska[1]

Received: 3 September 2020 / Revised: 23 November 2020 / Accepted: 3 December 2020 / Published online: 8 January 2021

Abstract

Current evidence indicates that resistance to the tyrosine kinase-type cell surface receptor (HER2)-targeted therapies is frequently associated with HER3 and active signaling via HER2-HER3 dimers, particularly in the context of breast cancer. Thus, understanding the response to HER2-HER3 signaling and the regulation of the dimer is essential to decipher therapy relapse mechanisms. Here, we investigate a bidirectional relationship between HER2-HER3 signaling and a type-1 transmembrane sorting receptor, sortilin-related receptor (SorLA; *SORL1*). We demonstrate that heregulin-mediated signaling supports SorLA transcription downstream of the mitogen-activated protein kinase pathway. In addition, we demonstrate that SorLA interacts directly with HER3, forming a trimeric complex with HER2 and HER3 to attenuate lysosomal degradation of the dimer in a Ras-related protein Rab4-dependent manner. In line with a role for SorLA in supporting the stability of the HER2 and HER3 receptors, loss of SorLA compromised heregulin-induced cell proliferation and sensitized metastatic anti-HER2 therapy-resistant breast cancer cells to neratinib in cancer spheroids in vitro and in vivo in a zebrafish brain xenograft model.

Introduction

The human epidermal growth factor receptor (HER) family is composed of four transmembrane receptor tyrosine kinases (RTKs), encoded by the *EGFR* (HER1) and *ERBB2-4* (HER2-4) genes. These receptors signal through homo- and heterodimerization and promote cell transformation and oncogenic properties in multiple cancer types, including breast cancer [1–3]. Much of the focus in this area has been on EGFR and HER2, which are well-established tumor drivers and targets of effective anti-cancer therapeutics [3, 4]. In contrast, the role of HER3 is less understood, and has until recently been underappreciated. This is largely owing to the fact that HER3 has impaired kinase activity and its phosphorylation depends on dimerization with other RTKs [1, 5]. However, an increasing number of studies acknowledge HER3 as a key driver of carcinogenesis due to its unique ability to directly activate the phosphatidylinositol-3-OH kinase (PI3K)/protein kinase B (AKT) signaling pathway. Moreover, HER3 dimerization with HER2, which has the strongest kinase activity among all HER proteins, represents the most potent signaling receptor pair within the HER family [2, 5–8].

HER3 drives resistance to targeted therapies in a wide range of solid tumors, including *ERBB2*-amplified (HER2-positive) breast cancer [5, 9, 10]. Increased HER3 expression compensates for HER2 tyrosine kinase inhibition, and HER3 activation by residual HER2 activity sustains oncogenic signaling [6, 7]. In addition, HER3 growth factor ligands, heregulins (a.k.a. neuregulins), mediate resistance to the anti-HER2 monoclonal antibody trastuzumab and the dual HER2/EGFR tyrosine kinase inhibitor lapatinib [11, 12]. Therefore, better management of the disease would require efficient and

Supplementary information The online version of this article (https://doi.org/10.1038/s41388-020-01604-5) contains supplementary material, which is available to authorized users.

✉ Hussein Al-Akhrass
hussein.al-akhrass@utu.fi

✉ Johanna Ivaska
joivaska@utu.fi

[1] Turku Bioscience Centre, University of Turku and Åbo Akademi University, FI-20520 Turku, Finland

[2] Danish Research Institute of Translational Neuroscience (DANDRITE) Nordic-EMBL Partnership, Department of biomedicine, Aarhus University, Aarhus, Denmark

safe targeting of the heregulin/HER2/HER3 signaling unit in tumors [5, 13]. However, so far, none of the reported anti-HER3 therapy clinical trials have resulted in Food and Drug Administration (FDA) approval in any cancer type [5].

Sortilin-related receptor (SorLA; *SORL1*) is a type-1 transmembrane sorting receptor that directs cargo proteins to spatially defined locations within the cell [14]. SorLA belongs to the family of vacuolar protein sorting 10 protein (VPS10P)-domain receptors [15], and is well characterized for its protective role in Alzheimer's disease, and for bolstering insulin signaling in adipose tissue, by regulating the traffic and biological function of the amyloid precursor protein and the insulin receptor, respectively [14, 16, 17]. The SorLA carboxy-terminal tail harbors different sorting motifs, which bind to cytosolic adapter proteins that regulate SorLA intracellular trafficking between the Golgi and the cell surface through endosomal compartments [18, 19]. The role of intracellular trafficking in the spatiotemporal regulation of EGFR signaling is well established [20, 21]. However, much less is known about the trafficking details influencing the oncogenic properties of HER2, or HER2-HER3 heterodimers [22]. We recently demonstrated that SorLA plays an important role in cancer, where it supports the oncogenic fitness of HER2 by orchestrating HER2 traffic to the plasma membrane, increasing signaling and proliferation in HER2-positive breast cancer [23].

This study aims to investigate the role of SorLA in mediating targeted therapy resistance in breast cancer, with a focus on the signaling by the HER2-HER3 oncogenic driver. We find that heregulins induce transcription of *SORL1* via HER2-HER3 signaling to the mitogen-activated protein kinase (MAPK) pathway. In addition, we demonstrate that SorLA supports HER2-HER3 expression in a Ras-related protein Rab4-dependent manner. Furthermore, we demonstrate, for the first time, that this regulation involves a direct SorLA interaction with the HER2-HER3 dimer. SorLA silencing inhibits 3D spheroid growth induced by heregulin-enriched stroma, and sensitizes metastatic breast cancer cells to the HER2/EGFR dual tyrosine kinase inhibitor neratinib in an in vivo xenograft model of brain tumors. This highlights SorLA as a potential target for the development of combination therapies aimed at overcoming HER3-mediated resistance of HER2-positive breast cancer patients to existing anti-HER2 therapies.

Results

Heregulins regulate *SORL1* expression

We stratified 59 breast cancer cell lines based on *ERBB3* or *ERBB2* expression by mining the publicly available Cancer Cell Line Encyclopedia (CCLE) database [24]. Our statistical analyses indicated significantly higher SorLA mRNA (*SORL1*) expression in high compared to low *ERBB3*- and *ERBB2*-expressing cells (Figs. 1A, S1A). In addition, *SORL1* expression was higher in tumors exhibiting high *ERBB3* and *ERBB2* expression (Fig. 1B; breast cancer patient data from the METABRIC study on the cBioportal database [25–27]). These findings suggested that HER2 and HER3 could positively regulate *SORL1* expression in breast tumors. To assess this hypothesis, we explored the effect of HER2-HER3 signaling on *SORL1* expression by stimulating BT-474 cells with heregulin β-1 (Hrg β-1) over a 72 h time course. Hrg β-1 treatment triggered an increase in SorLA protein levels in a time-dependent manner (Fig. 1C, D). As expected, it also activated AKT (AKT phosphorylation; pAKT) and the MAPK cascade (ERK phosphorylation; pERK) (Fig. 1C) [5]. The increase in SorLA correlated with elevated *SORL1* mRNA levels in Hrg β-1-treated BT-474 and MDA-MB-361 cells (Figs. 1E, S1B–D). These findings indicate that ligand-induced HER3 signaling positively regulates SorLA expression on the transcriptional level. In addition to exogenous Hrg β-1 ligand stimulation, autocrine ligand secretion in BT-474 cells, stably overexpressing Hrg β-1 (Fig. S1E), induced ERK and AKT phosphorylation (Fig. 1F), *SORL1* mRNA (Fig. S1F) and SorLA protein levels (Fig. 1F, G).

Hrg β-1 is an isoform resulting from alternative splicing events of *NRG1* gene transcripts [28]. To explore whether *SORL1* regulation is exclusive to Hrg β-1, we established a model of telomerase-immortalized foreskin fibroblasts (TIFF) with stable overexpression of SMDF (heregulin isoform 10), which exhibits neuronal functions [28] (Fig. S1G). We found that coculturing BT-474 cells with SMDF-TIFF significantly elevates SorLA levels and triggers AKT and ERK signaling in BT-474 cells (Fig. 1H, I). In addition, exposing BT-474 cells to conditioned medium from SMDF-TIFF significantly induced *SORL1* levels (Fig. S1H). This indicates that *SORL1* upregulation by HER3 signaling occurs both in a paracrine and in an autocrine manner, and is not restricted to a specific heregulin isoform. To further validate the role of HER2-HER3 in augmenting *SORL1* expression, we used an in vivo established model of brain-tropic metastatic BT-474 cells [29]. BT-474 cells from brain metastases (BT-474-Br) expressed significantly higher HER3 and HER2 levels, compared to the parental BT-474 cells, and this correlated with increased SorLA protein expression as well as *SORL1* transcription (Fig. 1J–L). Taken together, these results demonstrate that activation of HER2-HER3 positively regulates SorLA/*SORL1* expression in breast cancer.

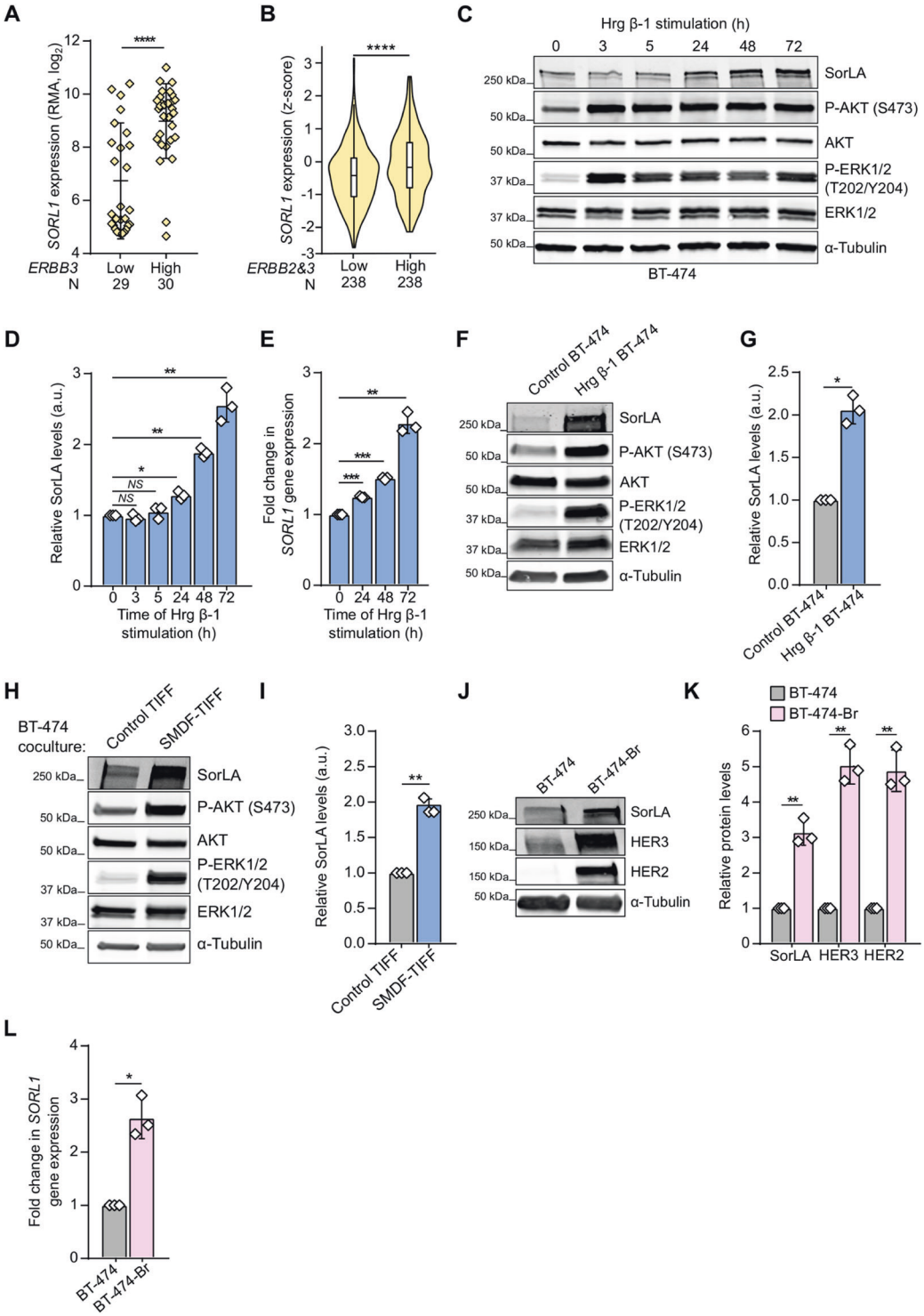

HER3 signaling to ERK1/2 upregulates *SORL1* expression

Next, we investigated the mechanistic details of heregulin-induced *SORL1* upregulation. We generated reporter constructs by placing a series of *SORL1* proximal promoter sequences in front of the firefly luciferase (Fig. 2A; P1-7). The P1-7 constructs were expressed individually in BT-474 cells, stimulated with Hrg β-1 for 24 h. Readouts of luciferase activity indicated that P3 is the minimum promoter sequence required for transcription in basal cell culture conditions (Fig. 2B). In addition, P3 exhibited the highest increase in luciferase activity upon Hrg β-1 stimulation (Fig. 2B), highlighting this region to contain responsive

◀ **Fig. 1 HER3 signaling regulates *SORL1* expression. A** *SORL1* expression is significantly higher in breast cancer cell lines with high *ERBB3* expression (CCLE; $N = 59$). RMA: robust multi-array average. Data are mean ± SD; statistical analysis: Mann–Whitney U. **B** *SORL1* expression is higher in tumors with high *ERBB3* and *ERBB2* expression (cBioPortal; $N = 476$). Violin plot boxes represent median and 25th and 75th percentiles (interquartile range), and whiskers extend to maximum and minimum values. See methods for details on how the groups were defined. **C** Hrg β-1 increases SorLA levels. BT-474 cells were stimulated with 20 ng.mL^{-1} Hrg β-1 for the indicated times. Representative immunoblotting of SorLA, AKT(p)S473, total AKT, ERK1/2(p)T202/Y204, total ERK1/2, with α-tubulin as a loading control. **D** Quantification of SorLA levels normalized to loading control and relative to non-stimulated (0 h) cells. **E** Hrg β-1 increases *SORL1* expression. Quantification of *SORL1* mRNA levels, relative to *HPRT1*, determined with RT-qPCR in BT-474 cells stimulated with 20 ng.mL^{-1} Hrg β-1 for the indicated time points relative to non-stimulated (0 h) cells. **F** Representative immunoblotting of SorLA, AKT(p)S473, total AKT, ERK1/2(p)T202/Y204, total ERK1/2, with α-tubulin as a loading control from control (mCherry)- or Hrg β-1-overexpressing BT-474 cells. **G** Quantification of SorLA levels normalized to loading control and relative to control cells. **H** SMDF increases SorLA expression. BT-474 cells were cultured on a monolayer of mCherry-positive control or SMDF-overexpressing fibroblasts (TIFF). BT-474 cells were FACS sorted (see "Methods") and cell lysates were analyzed for SorLA, AKT(p)S473, total AKT, ERK1/2(p)T202/Y204, total ERK1/2, with α-tubulin as a loading control. **I** Quantification of SorLA levels normalized to loading control and relative to control TIFF cocultured cells. **J** Representative immunoblotting of SorLA, HER2, and HER3, with α-tubulin as a loading control from parental BT-474 and brain-tropic metastasis variant BT-474-Br cells. **K** Quantification of indicated protein levels normalized to loading control and relative to BT-474 cells. **L** Quantification of *SORL1* mRNA levels, normalized to *HPRT1*, determined with RT-qPCR in parental BT-474 and BT-474-Br cells relative to BT-474 cells. Unless otherwise indicated, data are mean ± SD from three independent biological experiments; statistical analysis: Student's *t* test (unpaired, two-tailed, unequal variance).

elements to Hrg β-1 stimulation. To identify the intracellular signaling pathway responsible for Hrg β-1-mediated *SORL1* expression, we tested the ability of different signaling inhibitors to reduce Hrg β-1-induced P3 luciferase activity. The inhibitors were selected to specifically target individual proteins within the PI3K/AKT/mammalian target of rapamycin (mTOR) and ERK pathways known to be activated downstream of HER3 upon ligand stimulation [5]. Trametinib, an ERK pathway inhibitor, significantly decreased the Hrg β-1-induced luciferase activity of P3 (a similar trend was observed also with ERK kinase and ERK1/2 inhibitors selumetinib and SCH772984, respectively) (Fig. S2). In contrast, PI3K, AKT and mTOR inhibitors did not exhibit such effects on Hrg β-1-induced P3 activity (Fig. S2). This indicates that ERK signaling positively regulates the promoter activity of *SORL1* in response to Hrg β-1. In line with these luciferase promoter activity data, trametinib decreased GFP intensity in Hrg β-1-stimulated cells that express GFP under the control of the P3 promoter sequence (Fig. 2C, D). In addition, Hrg β-1-induced upregulation of SorLA protein in BT-474 cells was sensitive to trametinib, but not the AKT inhibitor MK-2206 (Fig. 2E, F), and trametinib inhibited *SORL1* mRNA expression in Hrg β-1-stimulated cells (Fig. 2G). Taken together these data uncover a previously unknown mechanism by which HER2-HER3 signaling to ERK1/2 regulates *SORL1* transcription leading to increased SorLA protein levels in breast cancer.

SorLA regulates HER3 stability

SorLA regulates HER2 stability in breast cancer [23]. Whether this regulation is exclusive to HER2 remained unknown. This prompted us to investigate the role of SorLA in regulating HER3 expression. We focused on HER3 since HER2-HER3 dimers control SorLA/*SORL1* expression (Fig. 1, 2) and drive therapy resistance in breast cancer [5, 6]. As a first exploratory analysis, we assessed whether SorLA and HER3 protein levels correlate using the quantitative proteomics of the CCLE on the DepMap portal database [30]. We found that SorLA and HER3 levels positively correlate across 29 breast cancer cell lines (Fig. 3A). To assess whether SorLA regulates HER3 in HER2-positive breast cancer, we expressed SorLA in JIMT-1 cells, which have very low endogenous SorLA expression compared to other HER2-positive cell lines [23]. Expression of SorLA increased HER3 levels significantly (Fig. 3B, C). Conversely, SorLA silencing in two endogenous SorLA-expressing HER2-positive cell lines, BT-474 and MDA-MB-361, with two different siRNAs significantly decreased HER3 expression (Figs. 3D, E; S3A, B). This indicates a regulation of HER3 by SorLA, in line with comparable effects of SorLA overexpression or silencing on HER2 levels (Figs. 3B–E; S3A, B), consistent with our previous findings [23].

To characterize the regulation of HER3 by SorLA in more detail, we performed qPCR analyses using our gain- and loss-of-function models. The expression of *ERBB3* remained unchanged upon SorLA overexpression or silencing, indicating that SorLA regulates HER3 at a post-transcriptional level (Fig. S3C). These results prompted us to test whether SorLA regulates HER3 stability. Cycloheximide (CHX) chase experiments revealed a significantly shorter HER3 half-life ($T_{1/2}$) in SorLA-silenced cells ($T_{1/2} = 4.5 \pm 1.6$ h) (Figs. 3F; S3D) compared to control-silenced cells ($T_{1/2} = 5.8 \pm 0.9$ h). Bortezomib-mediated inhibition of proteasome activity resulted in only a slight increase in HER3 levels, whereas, bafilomycin A1-mediated inhibition of lysosome function more than doubled HER3 protein levels (Fig. 3G, H), indicating that HER3 primarily undergoes lysosomal degradation in BT-474 cells. Moreover, the enhanced HER3 degradation, observed in CHX-treated SorLA-silenced cells, could be largely rescued by bafilomycin A1 treatment (Fig. 3I, J). Cumulatively, these data

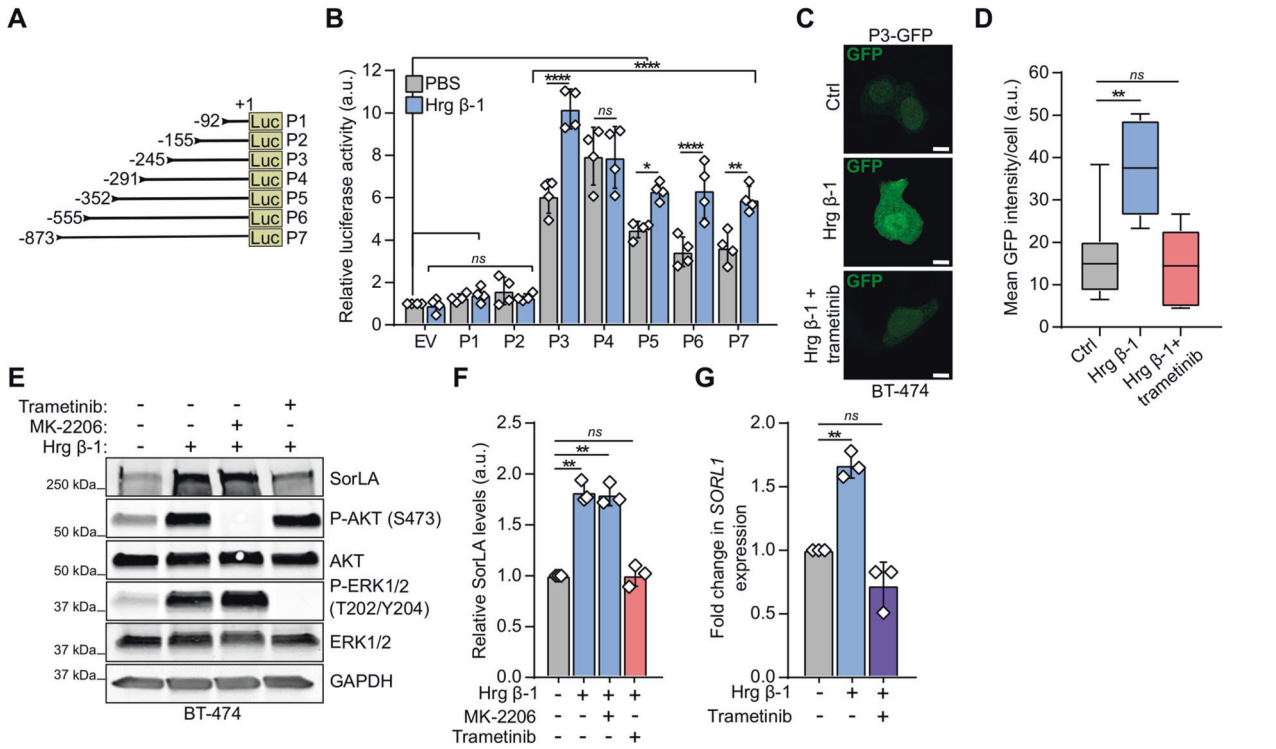

Fig. 2 Heregulin-induced *SORL1* regulation requires HER3 signaling through ERK1/2. A Representation of the different *SORL1* proximal promoter constructs (P1-7) used in luciferase assays with their corresponding molecular lengths (bp). **B** P3 is a responsive promoter sequence to Hrg β-1 stimulation. A control empty vector (EV) and P1-7 were individually expressed in BT-474 cells together with pRL-TK Renilla luciferase transfection control and cells were stimulated or not with 20 ng.mL^{-1} Hrg β-1 for 24 h. Shown are luciferase activities relative to the control sample (EV, PBS-treated). **C** Representative confocal microscopy images of P3-GFP promoter reporter construct-expressing BT-474 cells treated or not for 24 h with 20 ng.mL^{-1} Hrg β-1 in the presence or absence of 100 nM trametinib. Scale bars: 10 µm. **D** Quantification of the mean intensity of GFP signal per cell (whole-cell area). $N = 36$ cells per group. Three biological replicates. **E** Trametinib inhibits Hrg β-1-induced upregulation of SorLA. BT-474 cells were cotreated with 20 ng.mL^{-1} Hrg β-1 and either the pan-AKT inhibitor MK-2206 (2 µM) or the ERK pathway inhibitor trametinib (100 nM) for 48 h. Representative immunoblotting of SorLA, AKT(p)S473, total AKT, ERK1/2(p)T202/Y204, total ERK1/2, with GAPDH as a loading control. **F** Quantification of SorLA levels normalized to loading control and relative to non-treated cells. **G** *SORL1* mRNA levels, relative to *HPRT1*, determined with RT-qPCR in BT-474 cells stimulated or not with 20 ng.mL^{-1} Hrg β-1 in the presence or absence of trametinib relative to non-treated cells. Data are mean ± SD from four (**B**) and three (**F** and **G**) independent biological replicates; statistical analysis: (**B**) Two-way ANOVA, Dunnett's multiple comparisons test. (**F** and **G**) Student's *t* test (unpaired, two-tailed, unequal variance). (**D**) Box plots represent median and interquartile range, and whiskers extend to maximum and minimum values; One-way ANOVA, Dunn's multiple comparisons test.

implicate SorLA in attenuation of HER3 lysosomal degradation.

SorLA interacts with the HER2-HER3 dimer

Next, we aimed to explore whether the regulation of HER2 and HER3 stability is linked to SorLA association with the dimer. Bimolecular fluorescence complementation (BiFC) is a method to detect protein-protein interactions in live cells and is based on the reconstitution of a fluorescent protein (Venus in this study) via reassembly of two truncated, and nonfluorescent, N- (v1) and C-terminal (v2) fragments, fused to interacting proteins of interest [31] (Fig. 4A). Imaging of HER2-positive BT-474 cells coexpressing SorLA-v1 with either HER3-v2 or HER2-v2 revealed a strong, predominately intracellular fluorescent signal (Fig. 4B, insets 1-4), indicating the formation of SorLA-HER2 and SorLA-HER3 complexes in cells. HER2-HER3 (fused to v2 and v1, respectively) complexes were detected both at the cell surface and inside the cells (Fig. 4B, insets 5&6), demonstrating that HER2-HER3 heterodimers localize both to intracellular endomembrane-like structures and to the plasma membrane. To assess whether SorLA interacts with HER2-HER3 heterodimers, we used a conformation-specific nanobody to detect complemented Venus and to affinity purify the BiFC SorLA-HER3 complexes [32]. This biochemical approach revealed HER2 association with SorLA-HER3, indicative of the formation of a SorLA-HER2-HER3 trimeric complex in breast cancer cells (Fig. 4C). To determine whether SorLA interacts directly with the extracellular domains of HER2 and HER3, we performed

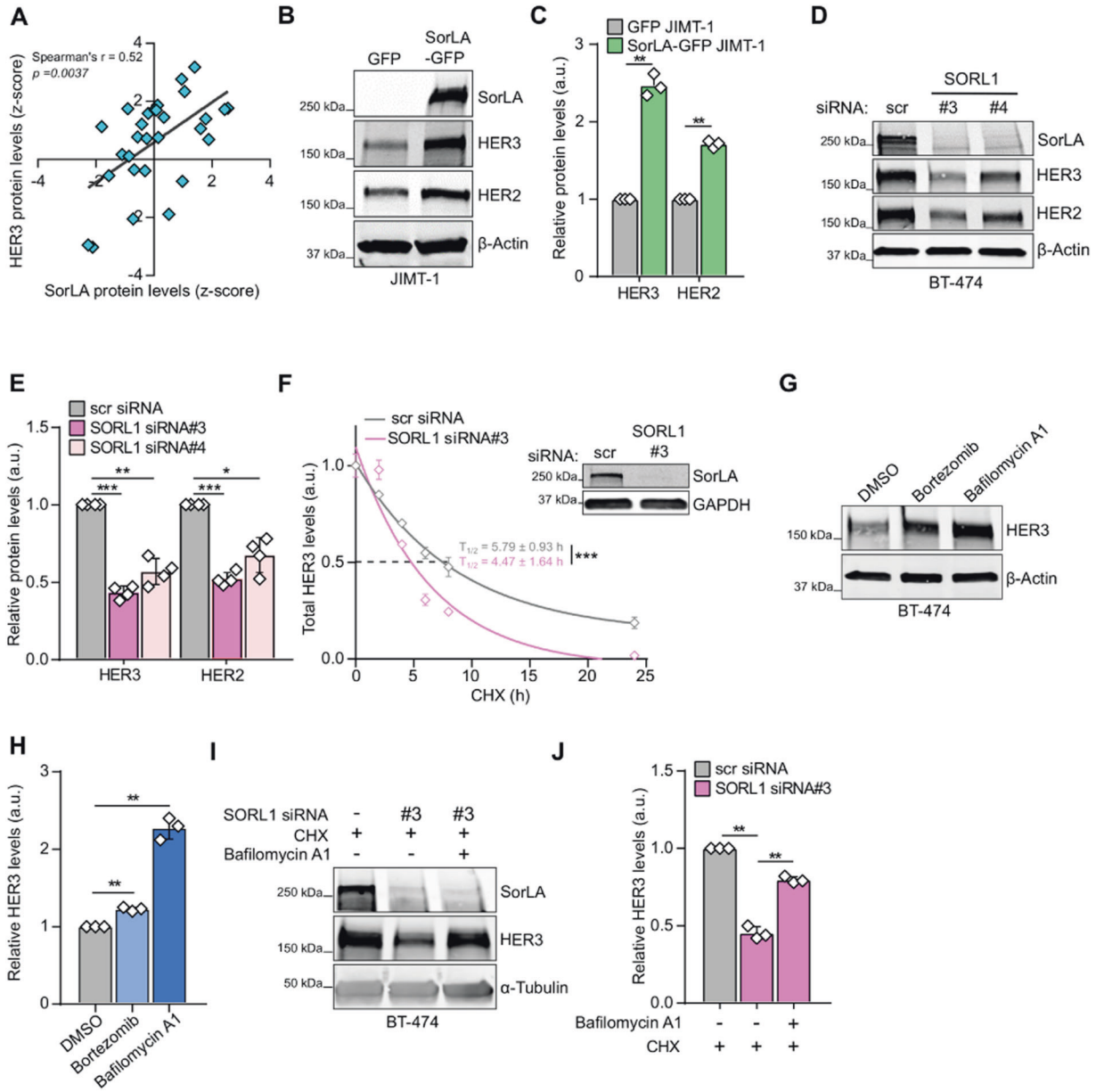

Fig. 3 SorLA regulates HER3 stability. A SorLA and HER3 protein levels correlate positively in breast cancer cell lines (DepMap portal; $N = 29$). **B**–**E** HER3 and HER2 expression correlates with SorLA in HER2-positive breast cancer. **B**, **C** SorLA-GFP transfection in JIMT-1 cells increases HER2 and HER3 levels compared to GFP transfected cells. **D**, **E**. SorLA silencing in BT-474 cells decreases HER2 and HER3. **B**, **D** Representative immunoblotting of total HER2, HER3, and SorLA with β-actin as a loading control. **C**, **E** represent the respective quantifications of immunoblots in (**B**, **D**) with HER2/HER3 levels normalized to loading control and relative to control-silenced cells. **F** SorLA silencing decreases HER3 stability. RNAi transfected BT-474 cells were treated with 25 $\mu g.mL^{-1}$ of CHX for the indicated time points and HER3 protein levels were determined by immunoblotting (see Fig. S3E). Shown are HER3 levels normalized to α-tubulin and relative to 0 h timepoint. Half-lives ($T_{1/2}$) represent the time required for HER3 to decrease to 50% of its initial level. The least squares fitting method and extra-sum-of-squares F test were used to assess the statistical difference between curves from control and SorLA-silenced cells ($P = 0.0002$). A representative western blot validating SorLA silencing is shown. **G** HER3 is primarily degraded through the lysosomal pathway. BT-474 cells were treated with 1 μM of bortezomib or 50 nM of bafilomycin A1 for 4 h to inhibit proteasome and lysosome activities, respectively. HER3 expression was analyzed by immunoblotting, with α-tubulin as a loading control. **H** Quantification of HER3 levels normalized to loading control and relative to DMSO-treated control cells. **I** SorLA silencing triggers HER3 lysosomal degradation. SorLA-silenced BT-474 cells were cotreated for 4 h with CHX and bafilomycin A1. HER3 expression was analyzed by immunoblotting, with α-tubulin as a loading control. **J** Quantification of HER3 levels normalized to loading control and relative to CHX-treated control-silenced cells. Data are mean ± SD from three (**C**, **F**, **H**, **J**) or four (**E**) independent biological replicates. Statistical analyses: Student's *t* test (unpaired, two-tailed, unequal variance) unless indicated otherwise. Scr: control non-targeting siRNA.

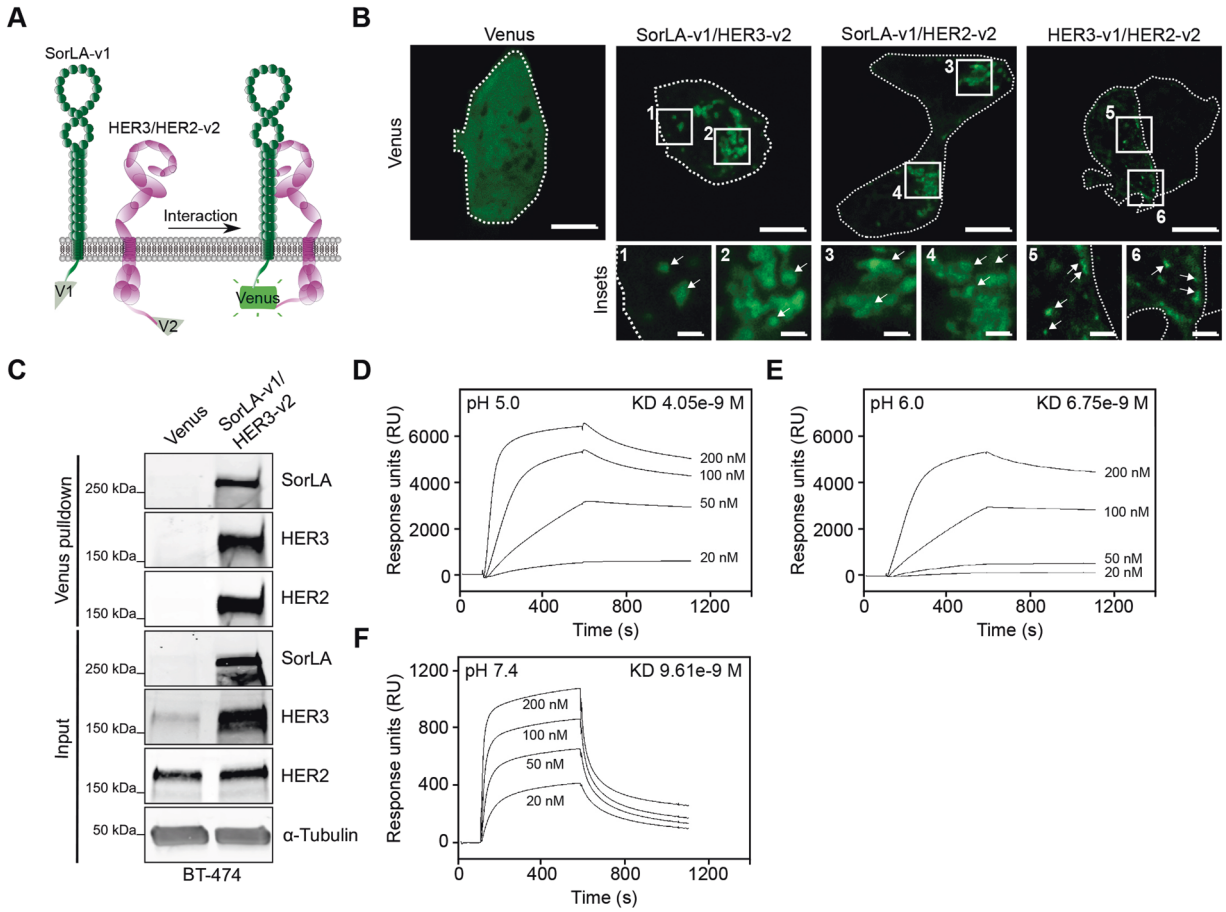

Fig. 4 SorLA interacts with HER2-HER3 dimers. A A scheme depicting BiFC between SorLA-v1 and HER2/3-v2. **B** The indicated BiFC dimers were expressed in BT-474 cells and their interaction was assessed through imaging of reconstituted Venus. Cells are outlined with white dotted lines. Shown are representative confocal microscopy images and a control Venus-expressing cell showing diffuse fluorescence localization. Scale bars (main): 10 µm. Scale bars (insets): 2 µm. **C** Venus or SorLA-v1/HER3-v2 were transiently expressed in BT-474 cells. Cell lysates were subjected to nanobody pulldown (specific for the reconstituted Venus v1 + v2 dimer) and pulldowns and total cell lysates (input) were immunoblotted with the indicated antibodies. **D–F**. SorLA interacts with HER3 in a pH-dependent manner. SPR analysis on immobilized SorLA and a 20–200 nM concentration series of HER3 at pH 5.0 (**D**), 6.0 (**E**) and 7.4 (**F**). KD: equilibrium dissociation constant. Data are representative of three independent biological replicates.

surface plasmon resonance (SPR) analysis, an assay that records protein interaction with an immobilized target on a microchip [33]. SPR analyses were performed using immobilized SorLA ectodomain under pH conditions corresponding to either endosomal (pH 5 & 6) or cell surface compartments (7.4) [34, 35]. Addition of the HER3 ectodomain at increasing concentrations triggered a rapid and reversible surge in binding (response units), indicating a specific interaction between SorLA and HER3 ectodomains (Fig. 4D). The strength of this interaction decreased with increasing pH (Fig. 4D–F), indicating that this interaction is pH-sensitive, similar to the interaction of SorLA with the amyloid precursor protein [36]. A similar interaction pattern was observed when increasing concentrations of the HER2 ectodomain were applied at different pH values (Fig. S4A–C). The kinetics of these interactions are given as supporting information (Supplementary Table 3). The SPR results demonstrate a previously unappreciated direct interaction of SorLA with both HER2 and HER3, and enhanced interaction at a lower pH, characteristic of endosomes [37].

SorLA regulates HER2 and HER3 stability in a Rab4-dependent fashion

SorLA regulates HER2 stability by supporting recycling of the receptor to the plasma membrane [23]. However, the mechanistic details of this process and its implications for HER3 remained to be determined. To investigate the trafficking pathway underpinning this regulation, we first assessed intracellular colocalization between GFP-SorLA and different RFP-tagged endosomal markers: early endosome antigen-1; vacuolar protein sorting-associated protein 29 (VPS29), a subunit of the retromer complex, which

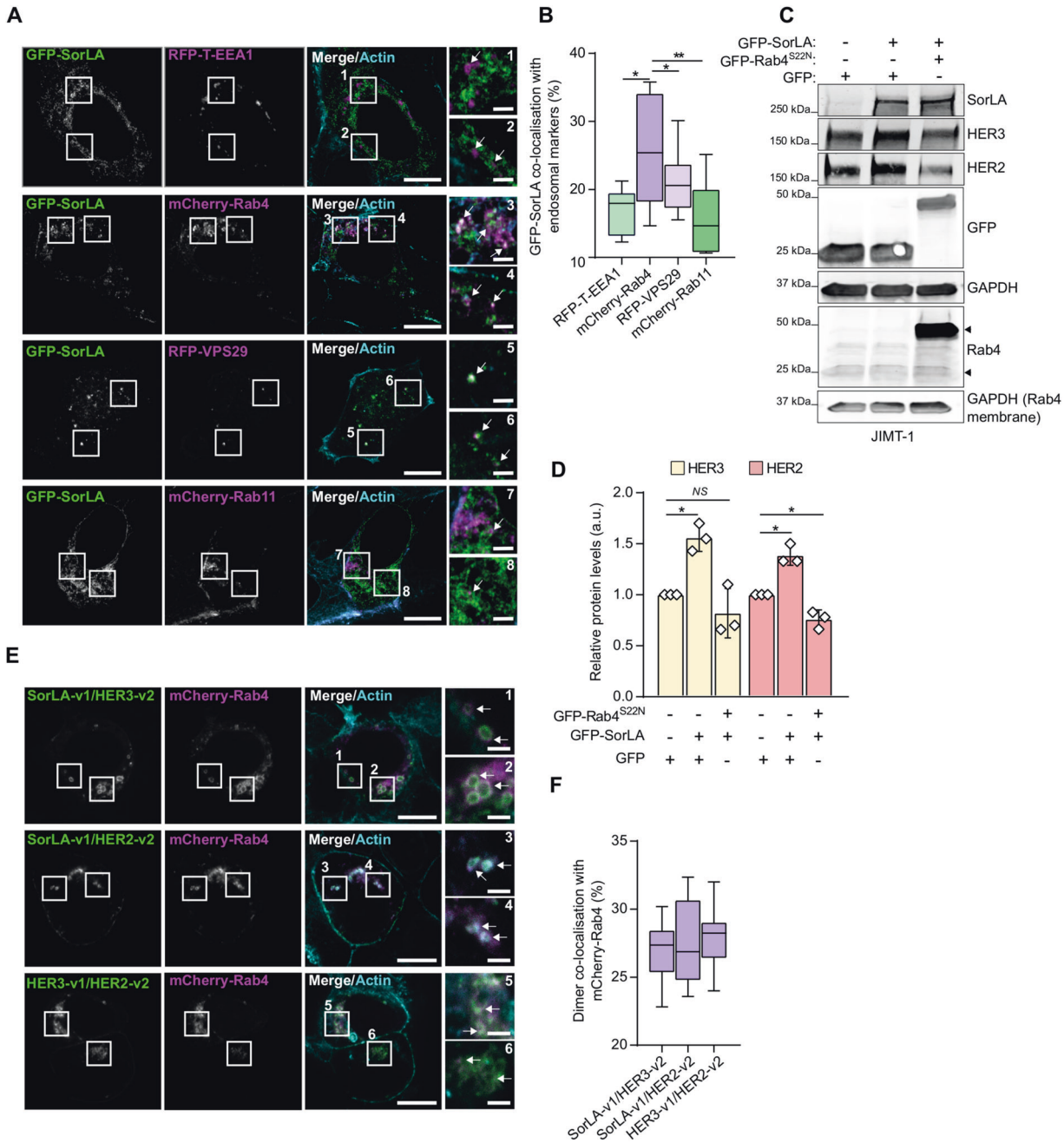

Fig. 5 SorLA regulation of HER2 and HER3 requires functional Rab4. A Representative Airyscan confocal microscopy images of BT-474 cells coexpressing GFP-SorLA with the indicated endosomal markers. SiR-Actin was used for counterstaining the actin cytoskeleton. White arrows depict colocalizing signals. Scale bars: 10 µm. Scale bars (insets): 2 µm. **B** GFP-SorLA strongly colocalizes with mCherry-Rab4 in BT-474 cells. Colocalization was calculated (see "Methods") from BT-474 cells transfected and imaged as in (**A**). $N = 36$ cells per group. **C** JIMT-1 cells were cotransfected with GFP-SorLA and either GFP control or GFP-Rab4^{S22N} dominant-negative mutant. Representative immunoblotting of SorLA, HER2, HER3, GFP, and Rab4, with α-tubulin as a loading control. GFP immunoblot detects GFP control and GFP-Rab4^{S22N} proteins. The higher molecular weight GFP-SorLA was probed with anti-SorLA primary antibody. In the Rab4 immunoblot, the upper arrowhead indicates GFP-Rab4^{S22N} and the lower arrowhead the endogenous protein. **D** Quantification of HER2 and HER3 levels normalized to loading control and relative to control GFP-transfected cells. **E** Representative confocal microscopy images of BT-474 cells co-overexpressing mCherry-Rab4 with the indicated BiFC dimers. SiR-Actin was used for counterstaining the actin cytoskeleton. White arrows depict colocalizing signals. Scale bars: 10 µm. Scale bars (insets): 2 µm. **F** Colocalization analysis between BiFC and mCherry-Rab4. $N = 30$ cells per group. **D** Data are mean ± SD from three independent biological experiments; statistical analysis: Student's t test (unpaired, two-tailed, unequal variance). **B** and **F** Box plots represent median and 25th and 75th percentiles (interquartile range), and whiskers extend to maximum and minimum values; three biological replicates. Statistical analysis: One-way ANOVA, Dunn's multiple comparisons test.

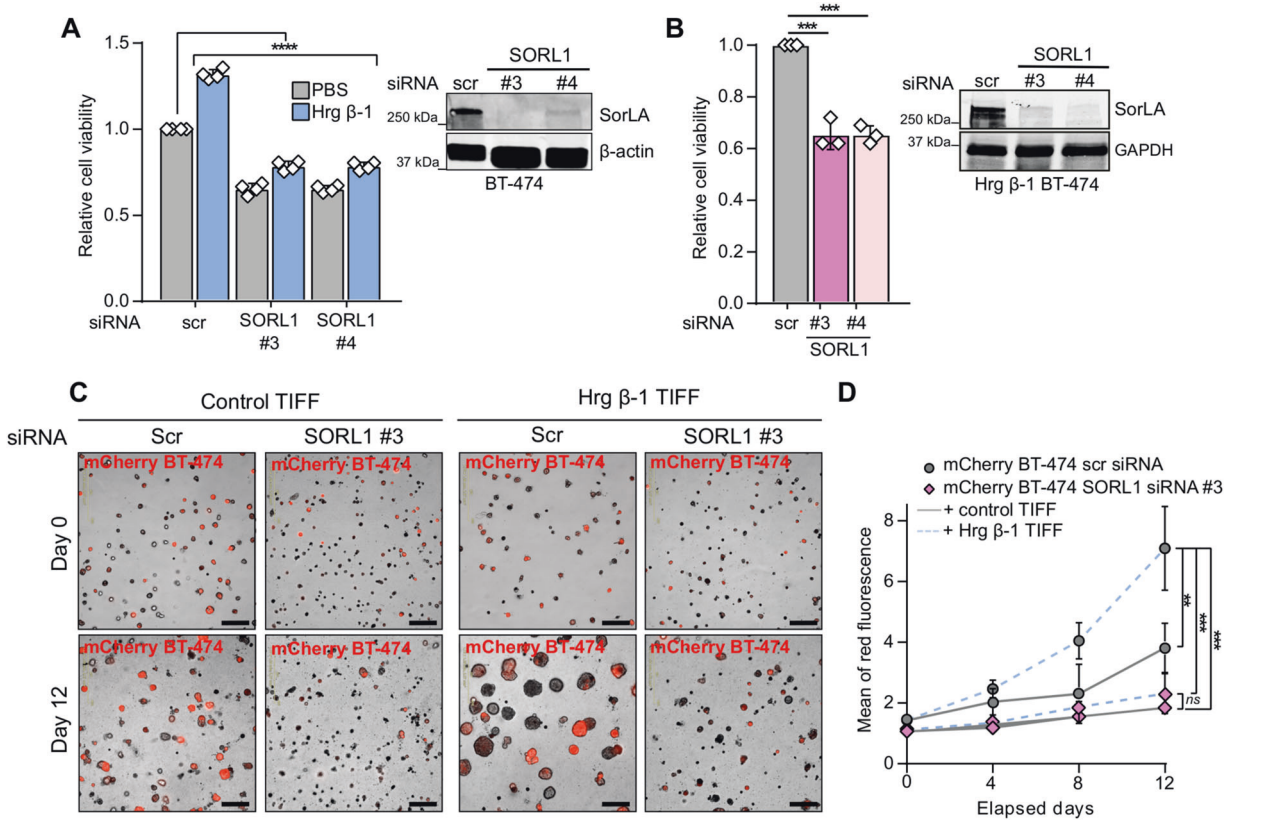

Fig. 6 SorLA expression determines heregulin response. A SorLA silencing decreases cell viability in basal and Hrg β-1-enriched cell culture conditions. Control and SorLA-silenced BT-474 cells were stimulated or not with 20 ng.mL^{-1} Hrg β-1 for 48 h and cell viability was assessed using a WST-8-based method. Cell viability values are represented as fold change relative to unstimulated control BT-474 cells. A representative western blot validating SorLA silencing is shown. **B** Hrg β-1-expressing BT-474 cells were silenced for SorLA and cell viability was analyzed as in (**A**). A representative western blot validating SorLA silencing is shown. **C**, **D** SorLA silencing inhibits spheroid growth in Hrg β-1-enriched extracellular matrix. SorLA-silenced mCherry BT-474 cells were cocultured with Hrg β-1-over-expressing fibroblasts (Hrg β-1 TIFF) in matrigel for 12 days. Shown are representative live-cell images (**C**) and quantification of mCherry fluorescence reflecting spheroid growth (**D**). Data are mean ± SD from three independent biological replicates; statistical analysis: (**A** and **D**), One-way ANOVA, Dunn's multiple comparisons test and (**B**), Student's *t* test (unpaired, two-tailed, unequal variance). Scr = control non-targeting siRNA.

mediates endosome-to-Golgi receptor retrieval [38]; and Rab4 and Rab11, which regulate receptor recycling from early endosomes and the endocytic recycling compartment, respectively [39]. Using confocal microscopy (Fig. S5A) and super–resolution Airyscan confocal microscopy (Fig. 5A), we readily detected overlapping signals between SorLA and the tested endosomal markers. Colocalization analysis indicated the highest degree of colocalisation between SorLA and Rab4 (Fig. 5A, insets3&4; Figs. 5B; S5A, insets3&4) indicating that SorLA may function in Rab4-containing recycling endosomes in BT-474 cells. Indeed, overexpression of a dominant-negative GDP-locked Rab4^{S22N} inhibited SorLA expression-induced up-regulation of HER2 and HER3 in SorLA-low JIMT-1 cells (Fig. 5C, D). This indicates that SorLA regulates HER2 and HER3 expression in a Rab4-dependent manner. In line with these results, we found that SorLA-, HER2- and HER3-containing BiFC dimers reside in Rab4-positive intracellular compartments in BT-474 cells (Fig. 5E, F), further highlighting the Rab4 pathway in mediating SorLA regulation of HER2-HER3 complexes in breast cancer.

SorLA is necessary for HER3-driven oncogenic cell growth

Our data thus far indicate a feed-forward loop between HER3 and SorLA where HER3 signaling induces SorLA expression and SorLA supports HER3 stability. Next, we evaluated the role of SorLA in the phenotype of HER3-driven cancer. Hrg β-1 stimulation resulted in enhanced cell viability in control-silenced BT-474 cells (Fig. 6A), whereas SorLA silencing resulted in diminished cell viability irrespective of Hrg β-1 stimulation (Fig. 6A). In addition, SorLA silencing, with two distinct siRNAs, inhibited the viability of Hrg β-1-expressing BT-474 cells (Fig. 6B). These data indicate that SorLA is required for Hrg β-1-induced cell viability in 2D cell culture.

Next, we investigated the role of SorLA in modulating heregulin effects within a more physiologically representative experimental setting. Control- and SorLA-silenced mCherry-BT-474 cells were cocultured as spheroids with either control or Hrg β-1-overexpressing fibroblasts, using a matrigel-based 3D culture system. While coculture with Hrg β-1-overexpressing TIFF strongly promoted the growth of control-silenced BT-474 spheroids, it had no effect on SorLA-silenced BT-474 spheroids (Fig. 6C, D). These results indicate that SorLA expression is essential for HER3-driven growth of tumor spheroids in heregulin-enriched stroma.

SorLA silencing sensitizes resistant cells to neratinib

Increased HER3 activation is implicated in resistance to targeted therapeutics against HER2, PI3K, and AKT in breast cancer [9, 10, 12]. Hence, we speculated that in such targeted therapeutic settings SorLA silencing might have a beneficial effect on drug response. We chose MDA-MB-361 cells as a model as they are derived from a HER2-targeted therapy-resistant brain metastasis [40] and their HER2 and HER3 levels are SorLA dependent (Fig. S3A, B). MDA-MB-361 cells were treated with either the pan-class I PI3K inhibitor buparlisib, the pan-AKT inhibitor MK-2206, or the dual HER2/EGFR tyrosine kinase inhibitor neratinib for 48 h (Fig. 7A, B). Consistent with its ability to inhibit *PIK3CA*-mutant p110α regulatory subunit of PI3K [41], buparlisib inhibited the viability of MDA-MB-361 control cells (Fig. 7A). In accordance with the partial sensitivity of MDA-MB-361 cells to AKT inhibitors [42], MK-2206 triggered a slight decrease in cell viability (Fig. 7A). No significant effect on cell viability was observed upon neratinib treatment of control MDA-MB-361 cells (Fig. 7B). SorLA silencing, with two different siRNAs, inhibited MDA-MB-361 cell viability in basal cell culture conditions (Fig. 7A, B) and SorLA silencing and neratinib exhibited synergistic inhibitory effects on MDA-MB-361 cell growth (Fig. 7B). We did not observe synergistic effects with buparlisib or MK-2206 (Fig. 7A) indicating that SorLA silencing specifically alters the response to neratinib. Since resistance to HER2 inhibition correlates with anchorage-independent growth [43], we analyzed growth of SorLA-silenced MDA-MB-361 spheroids in neratinib-containing ultra-low attachment cell culture conditions. Control MDA-MB-361 spheroids were resistant to neratinib, and these neratinib-treated cells were able to grow in the presence of Hrg β-1 (Fig. 7C, D). In contrast, SorLA silencing inhibited MDA-MB-361 spheroid growth, and the addition of neratinib further diminished the spheroid size even in spheroids treated with neratinib and Hrg β-1 (Fig. 7C, D), demonstrating that SorLA silencing alters neratinib sensitivity in spheroids and that SorLA is essential for inducing heregulin effects on cell growth. To determine whether loss of SorLA alters resistance to targeted therapy in vivo, we used a zebrafish model, an increasingly widely appreciated and powerful tool in cancer research [44]. GFP-labeled MDA-MB-361 cells, transiently silenced for SorLA expression, were engrafted in the brain of zebrafish embryos and the fish were then treated with buparlisib, neratinib or MK-2206. Neratinib treatment of SorLA-silenced cells resulted in regressed tumor growth while control tumors remained neratinib-resistant (Fig. 7E, F). In contrast, SorLA-silencing did not alter the response to buparlisib nor to MK-2206 (Fig. 7F). This highlights SorLA silencing as a sensitizing approach for HER2-targeted therapy, established here in MDA-MB-361 cells, but providing an essential proof-of-principle for future efforts to target SorLA as part of novel combination therapies.

Discussion

Here, we discovered a heregulin-dependent HER3 oncogenic signaling nexus, which forms the basis of a feed-forward loop supporting SorLA, HER2, and HER3 levels in breast cancer cells to drive neratinib resistance (Fig. 7G). We identified that heregulin-mediated signaling activates *SORL1* transcription *via* ERK-dependent induction of the *SORL1* promoter. In addition, we unraveled mechanistic details of HER3 regulation by SorLA. We found that SorLA interacts directly, and in a pH-sensitive manner, with the HER2-HER3 heterodimer to support receptor stability at the protein level. We detected this interaction in Rab4-positive endosomes, which appear to be crucial intracellular compartments for SorLA to divert HER2-HER3 from lysosomal degradation. Thus, we have uncovered a positive feedback mechanism whereby increased SorLA levels support HER2-HER3 dimer signaling to drive cell proliferation, anti-HER2 therapy resistance and further increase SorLA expression in cells.

Heregulins are a family of growth factors encoded by 6 individual genes (*NRG1-6*) with *NRG1* representing the archetypical growth factor ligand associated with poor prognosis in HER2-positive breast cancer [12, 28, 45]. The brain microenvironment is highly enriched with heregulins [10]. We found that the brain-tropic variants of BT-474 cells [29] exhibit increased SorLA/*SORL1* expression. This raises the possibility that SorLA may be relevant in breast cancer brain metastases. Heregulin affects cell proliferation in a cell-type specific manner. Hrg β-1 increases the proliferation of BT-474 cells at relatively low concentrations, while it exhibits a suppressive growth effect on MDA-MB-361 cells [46]. Despite this, the two cell lines showed a similar increase in SorLA/*SORL1* expression upon heregulin stimulation, and both autocrine and paracrine signals by various heregulin proteins increased SorLA/*SORL1* expression. This suggests that the regulation of SorLA, downstream of HER2-HER3 in response to heregulin-enriched tissue, is a general regulatory mechanism in breast cancer.

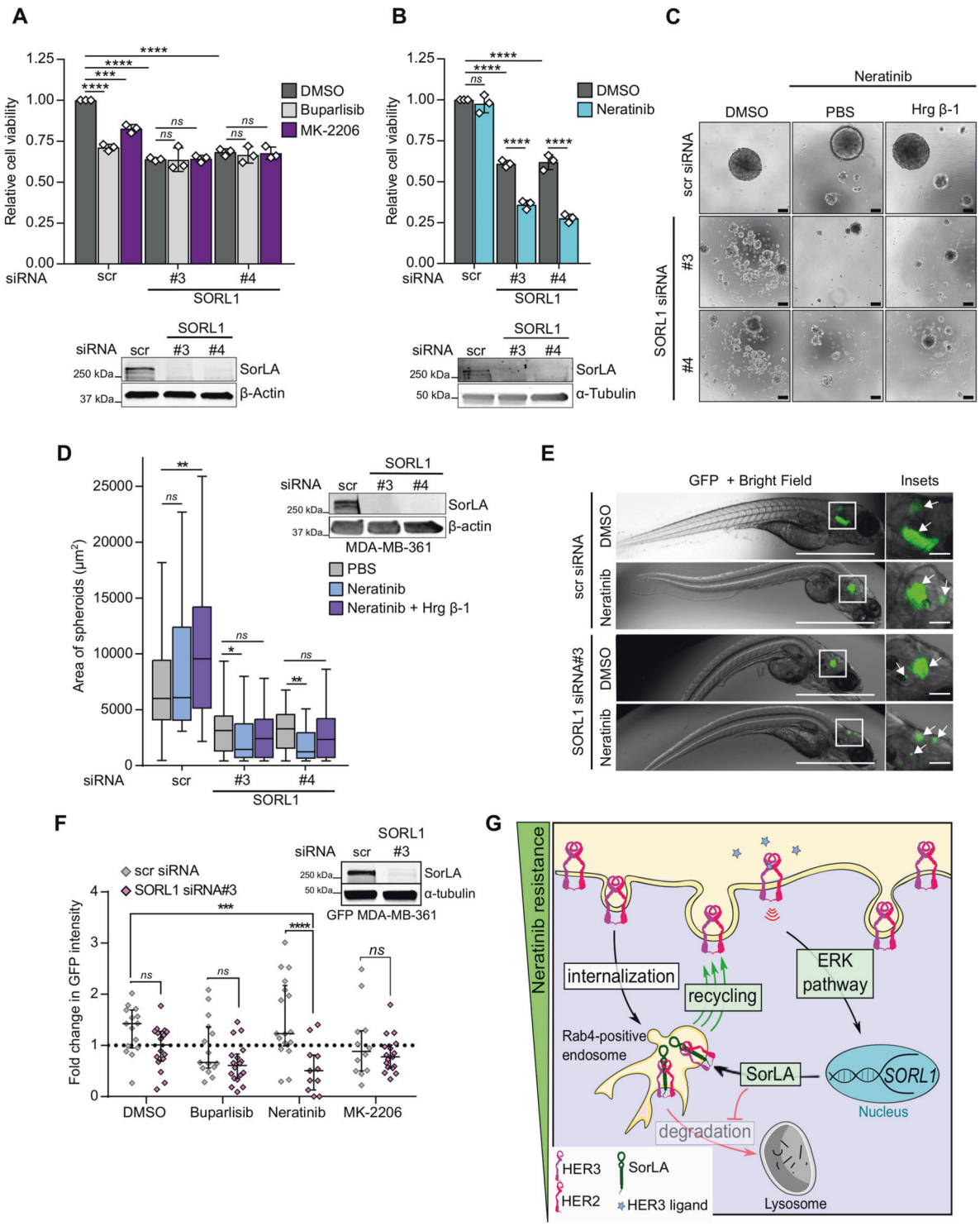

Our data indicate a Rab4-dependency of SorLA-mediated stabilization of HER2 and HER3. This would be in line with the role of Rab4 in mediating recycling of EGFR [47] and a recent study characterizing the role of altered Rab4-positive endosomes in sustaining EGFR signaling [48]. Nevertheless, the trafficking machinery linking SorLA to Rab4 remains to be investigated. The SorLA carboxy-terminal tail interacts with multiple trafficking proteins including GGA1 and GGA2 (Golgi-localizing, γ-adaptin ear homology domain, ARF-interacting proteins) [19]. GGA3 mediates Met RTK recycling from Rab4-positive endosomes [49] suggesting the possibility that members of the GGA family might influence SorLA-regulated RTK trafficking in HER2-positive breast cancer

◀ **Fig. 7 SorLA silencing specifically reverts resistance to neratinib in vitro and in vivo. A, B** SorLA silencing and neratinib show synergistic effects in inhibiting MDA-MB-361 cell growth. Control- and SorLA-silenced MDA-MB-361 cells were treated with either the pan-PI3K inhibitor buparlisib (500 nM), the pan-AKT inhibitor MK-2206 (500 nM) or the dual HER2/EGFR tyrosine kinase inhibitor neratinib (300 nM) for 48 h. Cell viability was measured using WST-8-based method. Values are represented as fold change relative to DMSO-treated control MDA-MB-361 cells. A representative western blot validating SorLA silencing is shown. **C**, **D** SorLA-silencing exhibits a synergistic effect with neratinib in inhibiting anchorage-independent spheroid growth of MDA-MB-361 cells in 3D low-attachment cell culture conditions. Control- and SorLA-silenced MDA-MB-361 cells were grown in low-attachment cell culture conditions for 7 days in the presence of the indicated treatments. Scale bar 100 µm. Spheroid sizes are quantified in and a representative western blot validating SorLA silencing are shown in (**D**). $N > 50$ spheroids per group. **E** Control and SorLA-silenced GFP-MDA-MB-361 cells were engrafted in the brain of zebrafish embryos and allowed to grow for 4 days in the presence of DMSO control or neratinib (400 nM). Representative GFP + Bright Field images of brain tumors are shown. Scale bars: 1 mm. Scale bars (insets): 100 µm. **F** Control- and SorLA-silenced GFP-MDA-MB-361 cells were engrafted in zebrafish brain and allowed to grow for 4 days in the presence of DMSO, buparlisib (2 µM), neratinib (400 nM) or MK-2206 (400 nM). Tumor growth is represented as fold change in GFP intensity relative to day 1 post-engraftment. A representative western blot validating SorLA silencing is shown. **G** A representative scheme of a neratinib resistance mechanism driven by a feed-forward loop supporting SorLA-HER2-HER3 expression. Key elements of this loop are highlighted in green boxes. HER2-HER3 signaling increases *SORL1* expression through the ERK pathway. Increased SorLA levels prevent HER2-HER3 lysosomal degradation (red arrow with lined arrowhead) presumably by stimulating receptor recycling from Rab4-positive endosomes (green arrows). Data are (**A** and **B**), mean ± SD from three 3 independent biological replicates; (**D**), Box plots representing median and interquartile range; whiskers extend to maximum and minimum values, and (**F**), median with interquartile range. Statistical analysis: (**A**, **B**), two-way ANOVA, Dunnett's multiple comparisons test. (**D**), One-way ANOVA, Dunn's multiple comparisons test. (**F**), two-way ANOVA, Dunnett's multiple comparisons test (main SorLA silencing effect $P < 0.0001$). Scr: control non-targeting siRNA.

cells. In addition, defining the interactome of SorLA in complex with RTKs, in an unbiased manner, might uncover key novel adapters/facilitators of SorLA-regulated traffic of receptors in cancer. Thus far, the role of SorLA in regulating oncogenic RTK signaling has been investigated in breast and bladder cancer [23]. Whether this mechanism is relevant for other cancer types remains to be investigated. For example, a related VPS10P-domain receptor, sortilin, promotes oncogenic growth in breast cancer [50, 51] but conversely attenuates EGFR signaling by enhancing its internalization and subsequent lysosomal degradation in lung cancer [20], suggesting that the biological roles of this family of proteins may be context and cancer type specific.

Our observation that heregulins upregulate SorLA and that SorLA, in turn, determines the heregulin response in BT-474 cells, alludes to a potential SorLA-dependent mechanism enabling metastatic breast cancer cells to adapt to, and colonize, the brain microenvironment. The heregulin-enriched brain parenchyma is known to promote resistance to anti-HER2 therapies enhancing the incidence of brain metastases that occurs in 50% of HER2-positive breast cancer patients [52–54]. Therefore, a molecular-level understanding of HER2-HER3 regulation in cells is required to not only dissect mechanisms of therapy relapse but to also provide alternative therapeutic options at such an advanced stage of the disease [5, 6, 10, 13]. A future therapeutic strategy undertaking an unbiased screening approach to identify potent SorLA blocking antibodies might provide a way forward in targeting heregulin-driven activation of the HER2-HER3 dimer in breast cancer. Our study demonstrates that SorLA silencing alters resistance of HER2-positive breast cancer cells to neratinib in the zebrafish heregulin-enriched brain microenvironment [55]. Neratinib is a dual HER2/EGFR tyrosine kinase inhibitor that was recently approved by the FDA for treatment of advanced or metastatic HER2-positive breast cancer [56]. We demonstrate that SorLA silencing exhibits a synergistic effect to neratinib, but not to buparlisib, or MK-2206. This might be linked to the ability of neratinib to induce ubiquitination and subsequent lysosomal degradation of HER2 [57]. Since SorLA silencing triggers HER2-HER3 lysosomal degradation, neratinib treatment could potentiate oncogenic-receptor targeting to the lysosomal pathway, a mechanism that does not apply to the other tested targeted chemotherapy agents. Given that HER3 drives therapy resistance and, despite extensive efforts, no anti-HER3 therapy is yet approved by the FDA [5], targeting key regulators of HER3 stability, such as SorLA, might reveal a new field of research for drug discovery.

This study is a significant conceptual advance to our previous findings initially linking SorLA to HER2 endosomal recycling. In summary, we describe an original role for SorLA as a positive regulator of the functional oncogenic driver HER2-HER3 in breast cancer. Since SorLA expression was associated with maintenance of anti-HER2 therapy resistance in brain metastasis xenografts, it may be a potential target for combating drug resistance. Additional research assessing the druggability of SorLA in breast cancer is warranted based on these findings.

Materials and methods

Cell culture and reagents

BT-474 (ATCC, HTB-20) and brain seeking BT-474-Br (generously provided by Dihua Yu (MD Anderson Cancer Center)) cells were grown in RPMI-1640 (Sigma-Aldrich, R5886) supplemented with 10% fetal bovine serum (FBS; Sigma-Aldrich, F7524), 1% vol/vol penicillin/streptomycin (Sigma-Aldrich, P0781-100ML) and L-glutamine. MDA-MB-361 cells were grown in Dulbecco's modified essential

medium (DMEM; Sigma-Aldrich, D5769) supplemented with 20% FBS, 1% vol/vol penicillin/streptomycin and L-glutamine. Telomerase immortalized foreskin fibroblasts (TIFF, generously provided by J. Norman (Beatson Institute for Cancer Research)) and JIMT-1 (DSMZ, ACC 589) cells were grown in DMEM supplemented with 10% FBS, 1% penicillin/streptomycin and L-glutamine. All cells were cultured in a humidified incubator set at 5% CO_2 and 37 °C. All cells were tested bimonthly – every 2 months – to ensure mycoplasma-free cell culture using MycoAlert™ mycoplasma detection kit (Lonza, #LT07-418) and MycoAlert™ assay control set (#LT07-518). Cell lines were not separately authenticated within this study. The antibodies used are described in Supplementary Table 1. Previously published plasmids used in this study are summarized in Supplementary Table 2.

Western blot

Cells were washed with ice-cold Dulbecco's phosphate-buffered saline (DPBS, Gibco™, 11590476) prior to lysis with cell lysis buffer (CST, #9803) supplemented with 1% protease/phosphatase inhibitor cocktail (CST, #5872). Cell lysates were sonicated and cleared by centrifugation at 18,000 × *g* for 10 min. Unless otherwise indicated, 30 µg of cleared lysates were subjected to SDS-PAGE under denaturing conditions (4–20% Mini-PROTEAN TGX Gels) and were transferred to nitrocellulose membranes (Bio-Rad Laboratories). Membranes were blocked with 5% milk-TBST (Tris-buffered saline and 0.1% Tween 20) and incubated with the indicated primary antibodies overnight at +4 °C. Primary antibodies were diluted in blocking buffer (Thermo, StartingBlock (PBS) blocking, #37538) and PBS (1:1 ratio) mix and incubated overnight at +4 °C. After primary antibody incubation, membranes were washed three times with TBST and incubated with fluorophore-conjugated secondary antibodies diluted (1:2000) in blocking buffer at room temperature for 1 h. Membranes were scanned using an infrared imaging system (Odyssey; LI-COR Biosciences). The following secondary antibodies were used: donkey anti-mouse IRDye 800CW (LI-COR, 926-32212), donkey anti-mouse IRDye 680RD (LI-COR, 926-68072), donkey anti-rabbit IRDye 800CW (LI-COR, 926-32213) and donkey anti-rabbit IRDye 680RD (LI-COR, 926-68073). The band intensity of each target was quantified using ImageJ (NIH) [58] and normalized to loading control band intensity in each lane.

Venus pull-down

Cells were lysed in Pierce IP Lysis Buffer (Thermo Scientific, 87787) supplemented with 1% protease/phosphatase inhibitor cocktail (CST, #5872). Lysates were cleared by centrifugation at 18,000 × *g* for 10 min. 5% of cleared lysates were used as input control. Cleared lysates were incubated with GFP-trap beads (Chromotek, gtak-20) for 50 min at +4 °C to pull-down Venus-tagged proteins. Venus-trap beads were then pelleted by centrifugation at 3000 rpm for 3 min and washed 3 times with an IP wash buffer (20 mM tris-HCl (pH 7.5), 150 mM NaCl, 1% NP-40). Finally, pellets were boiled at 95 °C for 10 min in sample buffer prior to SDS-PAGE.

Quantitative reverse transcription-PCR

Total RNA was extracted according to the manufacturer's instructions (NucleoSpin RNA extraction kit, Macherey −Nagel, 740,955.5). RNA concentration was measured by NanoDrop Lite (Thermo). Single-stranded cDNA was prepared using the high capacity cDNA reverse transcription kit (Applied Biosystems). The reaction was stopped by incubation at 95 °C for 5 min. Approximately 100 ng of cDNA was used for each PCR reaction performed with TaqMan probes according to the manufacturer's instructions (Thermo/Applied Biosystems, TaqMan™ Universal Master Mix II, 4440040). The following TaqMan probes were used: SORL1 (Hs00268342_m1), ERBB3 (Hs00176538_m1), NRG1 (Hs00247624_m1) and HPRT1 (Hs02800695_m1). NRG1 primers recognize both Hrg β-1 and SMDF splicing variants of *NRG1* gene transcripts. Relative quantification of gene expression values was calculated using the ΔΔCt method [59].

Transient transfections

For transient overexpression, cells were transfected 24 h before experiments using Lipofectamine 3000 (Invitrogen, P/N 100022052) and P3000 enhancer reagent (Invitrogen, P/N100022058) according to the manufacturer's instructions. For interference assays, cells were transfected 72 h before experiments using Lipofectamine RNAiMAX reagent (Invitrogen, P/N 56532) according to the manufacturer's instructions. SORL1-targeting siRNAs were obtained from Dharmacon – siSORL1 #3 (J-004722-07, (5'CCGAAGAGCUUGACUACUU3')), siSORLA #4 (J-004722-05, (5'CCACGUGUCUGCCCAAUUA3')). Allstars (Qiagen, 1027281) was used as a negative control. All siRNAs were used at a final concentration of 20 nM.

Cell viability assays

Cells were silenced for SorLA in 6-well plates and then replated on 96-well plates (5000 cells/well) in a volume of 100 µL and allowed to grow for 72 h. After experiments, 10 µL/well of WST-8 (cell counting kit 8, Sigma-Aldrich, 96992) reagent was added. After 3 h of incubation at 37 °C

with 5% CO_2, absorbance was read at 450 nm (Thermo, Multiscan Ascent). Medium without cells was used as a background control, subtracting this from the sample absorbance readings. Cell viability was calculated as a ratio of endpoint absorbance relative to control cells.

Treatments

Heregulin β-1 (Sigma, H7660) was used at a working concentration of 20 ng.mL^{-1}. For lysosome and proteasome inhibition, cells were treated for 4 h with 50 nM of bafilomycin A1 (Calbiochem, 196000) and 1 μM of bortezomib (Adooq Bioscience, A10160), respectively. CHX (Sigma, 01810) was used for translation inhibition at 25 μg.mL^{-1}. For targeted inhibition of intracellular signaling proteins, trametinib (Adooq Bioscience, JTP-74057, [100] nM), rapamycin (Santa Cruz Biotechnology, sc-3504A, [100] nM), buparlisib (Adooq Bioscience, AT11016, [500 nM]), selumetinib (Adooq Bioscience, A10257, [1 μM]), SCH772984 (Adooq Bioscience, A12824, [1] μM) and MK-2206 (Adooq Bioscience, A10003, [2] μM) were used for the indicated time points.

Immunofluorescence and confocal microscopy analyses

Cells were plated on μ-Slide 8-well dishes (Ibidi, 80826) and washed twice with ice-cold PBS before fixation in 4% paraformaldehyde for 10 min on ice. After fixation, cells were washed and then incubated with a permeabilization buffer (1X PBS/5% horse serum/0.3% Triton™ X-100) for 60 min. SiR-actin (Tebu-Bio, SC001) was used for counterstaining the cytoskeletal actin. Images were obtained using Zeiss LSM880 laser scanning confocal microscope. Airyscan images were processed with an Auto processing strength. Quantification of colocalization between SorLA and endosomal markers was performed using the ImageJ [58] plugin ComDet (https://github.com/ekatrukha/ComDet) [60].

Dual-luciferase reporter assays

Firefly and *Renilla* luciferase activities of the same sample were sequentially measured with the results expressed as the ratio of firefly to *Renilla* luciferase activity. 3×10^4 Cells were seeded per well of 48-well plates. Cells were cotransfected with 5' *SORL1* proximal promoter fragments in pGL4.10[luc2] vector (Promega, E6651) and pRL-TK *Renilla* control reporter vector (Promega, E2241) at relative DNA amounts of 95 and 5%, respectively. After the indicated treatments, cells were lysed and luciferase assays were performed using the Dual-Luciferase® Reporter Assay System (Promega, E1980) according to the manufacturer's instructions. Luciferase activity was measured using Synergy H1 Hybrid Reader (BioTek). Each value of luciferase activity represents the mean of three internal replicates.

Cell sorting

BT-474 cells were cultured on a monolayer of mCherry- or heregulin isoform 10 (SMDF)-overexpressing fibroblasts for 36 h. To bypass antibody-labeling steps prior to cell sorting, mCherry was overexpressed in BT-474 cells before starting the coculture with SMDF-overexpressing fibroblasts. Before sorting, cells were detached using trypsin, harvested and put immediately on ice. Positive and negative selection of BT-474 cells was applied based on mCherry signal using Sony SH800S cell sorter. BT-474 cells were then pelleted and lysed in cell lysis buffer (CST, #9803) supplemented with 1% protease/phosphatase inhibitor cocktail (CST, #5872) prior to SDS-PAGE.

Anchorage-independent 3D spheroid formation assays

An adapted protocol from [61] was used for spheroid growth assays. Cells were counted and equal amounts were plated in ultra-low attachment 96-well plate (Corning, CLS3474-24EA). Cells were allowed to proliferate for 7 days. Three internal replicates were plated for each sample. Images of spheroids were acquired using Eclipse Ti2 inverted microscope (Nikon) and spheroid volume was calculated using ImageJ (NIH).

Matrigel-based multi-spheroid 3D growth assays

The bottom wells of a μ-Plate 96 well plate (ibidi, 89646) were filled with 10 μL of 50% matrigel (Corning, 356231) then the plate was centrifuged at 200 × *g* for 20 min. The coated plate was incubated at 37 °C for 30 min. Wells were then filled with 20 μL of cell suspension (1000 cells, 1:1 ratio of BT-474 cells to TIFF) in 25% matrigel and incubated overnight at 37 °C. Wells were then filled with 65 μL of cell culture medium that was replaced every 2 days. Wells were imaged using the IncuCyte® S3 instrument (sartorius) and spheroid growth, reflected by mCherry fluorescence, was analyzed using the IncuCyte software (sartorious).

Cloning for pLenti-SorLA-C-GFP and bimolecular fluorescence complementation (BiFC)

SORL1 ORF was ordered from Origene in the pLenti-C-Myc-DDK plasmid (Origene, PS100064). The SORL1 ORF was digested using EcoRI and XhoI and ligated into the

pLenti-C-GFP plasmid (Origene, PS100065) between EcoRI and XhoI restriction sites. pDEST-SorLA-v1 (Addgene, #154892) was generated by first PCR amplifying the SorLA coding sequence from the pLenti-SorLA-C-GFP vector using the primers 5'-GGTACTCGAGGCCACCatggcgacacggagcagcaggaggga-3' and 5'-GGTCGAATTCggctatcaccatggggacgtcatctgaaaatccag-3'. PCR fragments were then subcloned into the pDEST-ORF-v1 (a kind gift from Darren Saunders, Addgene, #73637) [32] vector using the XhoI/EcoRI restriction enzymes. For the pDEST-ERBB2-v2 (Addgene, #154895), pDEST-ERBB3-v1 (Addgene, #154893) and pDEST-ERBB3-v2 (Addgene, #154894) vectors, LR reactions (LR clonase II, ThermoFisher Scientific) were performed using the pDEST-ORF-v1 and pDEST-ORF-v2 (Addgene, #73638) [32] destination vectors, and pDONR223-ERBB2 (a kind gift from William Hahn & David Root, Addgene, #23888) [62] and pDONR223-ERBB3 (Addgene, #23874) [62] shuttle vectors. pENTR2b-mVenus was LR subcloned into pEF.DEST51 (ThermoFisher Scientific, #12285011) to generate the expression plasmid, pEF.DEST51-mVenus. All vectors were verified by analytical digests and sequencing.

Lentivirus-mediated overexpression of Hrg β-1 and SMDF

Hrg β-1- and SMDF-coding sequences were LR subcloned from pENTR(tm)221 shuttle vectors (ThermoFisher Scientific Ultimate™ ORF, IOH80996, IOH80996) into pLenti6.3/V5-DEST (ThermoFisher Scientific, V53406) to generate expression plasmids. Lentiviral particles were generated in the 293FT packaging cell line (complete medium: high glucose DMEM, 10% FBS, 0.1 mM NEAA, 1 mM MEM Sodium Pyruvate, 6 mM L-Glutamine, 1% Pen/Strep and 0.5 mg/ml Geneticin) by transient transfection of transfer vector, either pLenti6.3/v5-DEST-SMDF (SMDF) or pLenti6.3/V5-DEST-Hrg β-1 (Hrg β-1), 2nd generation packaging plasmid-psPAX2 and envelope vector-pMD2 (kind gifts from Didier Trono, Addgene plasmids #12259 and #12260, respectively) with the ratio (7:2:1) using calcium-phosphate precipitation method [63]. 72 h post transfection medium containing viral vectors was collected, concentrated for 2 h by ultracentrifugation in a swing-out rotor SW-32Ti (Beckman Coulter, Brea, US-CA) at $26000 \times g$, resuspended in residual medium and flash frozen in liquid nitrogen. Functional titer of ~1×10^8 was measured in 293FT cells by FACS (BD LSRFortessa, Becton Dickinson). For stable overexpression, 8×10^4 BT-474 cells and TIFF were seeded in a 24-well plate, 24 h later cells were transduced with MOI 1, 2, and 4 of Hrg β-1 or SMDF lentiviral stocks in low volume of full media. Medium containing viral particles was removed 16 h later. After 4 days, antibiotic selection was initiated with 35 µg/ml Blasticillin. Five days later, the selection was terminated. The MOI 4 condition with the highest (*ca.* 40%) survival rate was chosen for further experiments after validation of *NRG1* overexpression by qPCR.

Zebrafish experiments

Zebrafish embryo experiments were carried out under license ESAVI/9339/04.10.07/2016 (National Animal Experimentation Board, Regional State Administrative Agency for Southern Finland). No randomization or blinding was carried out since it was not applicable to our study. To test toxicity of tested drugs, 2dpf zebrafish embryos of casper strain [64] were cultured in 96-well plates (1 embryo/well) and exposed to concentration series of tested drugs. All wells had a final concentration of 1% of DMSO and E3 + PTU medium (5 mM NaCl, 0.17 mM KCl, 0.33 mM $CaCl_2$, 0.33 mM $MgSO_4$, 0.2 mM 4-phenylthiourea) at 33 °C. After 2 days of incubation, the mortality of embryos was evaluated under a stereomicroscope. The surviving embryos of each drug concentration were pooled, lysed for protein extraction and subsequently subjected to western blot analysis of biomarker proteins. For each drug, a lowest effective concentration resulting in robust decrease in biomarker was selected to be used in the following xenograft experiments.

Zebrafish embryo xenograft studies were essentially carried out as described in detail earlier [65]. In short, one day prior to transplantation GFP-MDA-MB-361 cells were transfected with control or SORL1 siRNAs. On the next day, the 2 dpf zebrafish embryos were immobilized in agarose, tumor cells suspended in PBS and injected into the brain from the dorsal side. One day post injection (1 dpi), successfully transplanted embryos were placed in CellView glass bottom 96-well plate (1 embryo/well) and drug treatments were initiated and embryos incubated in E3 + PTU at 33 °C. The xenografted embryos were imaged using a Nikon Eclipse Ti2 fluorescence microscope and a 2x Nikon Plan-Apochromat (NA 0.06) objective. Each embryo was imaged both at 1dpi and 4 dpi using brightfield illumination and a GFP fluorescence filter set (excitation with 470 nm LED). Each image was inspected manually to filter out severely malformed, dead or out of focus embryos. Next, the tumor area was measured using ImageJ (NIH). The fold change in tumor size was calculated in below equation:

$$\text{Fold change} = (\text{GFP intensity}\,(4\text{dpi}))/(\text{GFP intensity}\,(1\text{dpi})). \quad (1)$$

SPR analysis

SPR analysis was carried out by using a BIAcore3000 system (BIAcore, Uppsala). The SorLA

ectodomain [16] was immobilized on a CM5 chip at a density of 56 fmol/mm^2. Subsequently, a concentration series of HER3 (ACRO Biosystems, ER3-H5223) or HER2 (ACRO Biosystems, HE2-H5212) were applied to the chip surface in 10 mM Hepes, pH 7.4/150 mM NaCl/5 mM $CaCl_2$/0.005% Tween 20, and the respective BIAcore signals were expressed in RU corresponding to the difference in response between SorLA-coated and un-coated control flow channel. Kinetic parameters were determined by BIAEVALUATION 4.1 software.

In silico analyses

SORL1, *ERBB2*, and *ERBB3* gene expressions in breast cancer cell lines were curated from the CCLE [24]. The median gene expression was used to divide the dataset into high (above median) and low (below median) *ERBB2*- or *ERBB3*-expressing cells, and *SORL1* expression was analyzed in each group. *SORL1*, *ERBB2*, and *ERBB3* gene expressions in breast tumors was curated from the METABRIC study publicly available on the cBioportal database [25–27]. The median *ERBB2* expression was used to divide the cohort into high (above median) and low (below median) *ERBB2*-expressing tumors. The resulting subgroups were further split based on *ERBB3* expression using the quartile method, with high *ERBB2&3*-expressing tumors being the upper *ERBB3* quartile in *ERBB2*-high tumors, and the low *ERBB2&3*-expressing tumors representing the lower *ERBB3* quartile in *ERBB2*-low tumors. *SORL1* expression was compared between high and low *ERBB2&3*-expressing samples. The protein levels of SorLA and HER3 in breast cancer cell lines were curated from the Depmap portal database [30] and the dataset was subjected to a linear regression analysis.

Statistical analyses

At least three independent biological replicates were performed for each experiment. The sample size (N) and the related statistical methods are described within figure legends. When data deviated from a normal distribution based on the D'Agostino-Pearson normality test, non-parametric statistical tests were used. Significance was concluded when a probability value (P value) was lower than 0.05. NS: not significant; $*P < 0.05$; $**P < 0.01$; $***P < 0.001$; $****P < 0.0001$. In every case, unequal variances between groups of data were assumed and two-tailed P values were reported. No power analyses were conducted to estimate sample sizes.

Data availability

The authors declare that the data supporting the findings of this study are available within the article and from the authors on request.

Acknowledgements We thank J. Siivonen and P. Laasola for technical assistance. H. Hamidi is acknowledged for illustrations and editing of the manuscript. The Ivaska laboratory is acknowledged for lively discussions and critical feedback on the manuscript. Guillaume Jacquemet, Jukka Westermarck, Majid Momeny, and Patrick Brest are acknowledged for critical reading of the manuscript. The Cell Imaging and Cytometry and Genome Editing core facilities (Turku Bioscience Centre, University of Turku and Åbo Akademi University and Biocenter, Finland); the EuroBioimaging node in Turku and the Zebrafish core facility (Turku Bioscience Centre, University of Turku and Åbo Akademi University) are acknowledged for services, instrumentation, and expertise. This study was supported by the Academy of Finland (J. Ivaska grant 312517), the Academy of Finland CoE for Translational Cancer Biology (J. Ivaska), the European Research Council CoG grant 615258 (J. Ivaska), the Sigrid Juselius Foundation (J. Ivaska) and the Finnish Cancer Organization (J. Ivaska). H. Al-Akhrass has been supported by the Finnish Cultural Foundation Central Fund 190150. J.R.W. Conway has been supported by the European Union's Horizon 2020 research and innovation program under Marie Sklodowska-Curie grant agreement 841973. O.M. Andersen has been supported by The Independent Research Fund Denmark grant DFF-4004-00371. J. Kaivola has been supported by TuDMM Doctoral Program, University of Turku.

Compliance with ethical standards

Conflict of interest The authors declare that they have no conflict of interest.

Publisher's note Springer Nature remains neutral with regard to jurisdictional claims in published maps and institutional affiliations.

References

1. Junttila TT, Akita RW, Parsons K, Fields C, Lewis Phillips GD, Friedman LS, et al. Ligand-independent HER2/HER3/PI3K complex is disrupted by trastuzumab and is effectively inhibited by the PI3K inhibitor GDC-0941. Cancer Cell. 2009;15:429–40.
2. Vaught DB, Stanford JC, Young C, Hicks DJ, Wheeler F, Rinehart C, et al. HER3 is required for HER2-induced preneoplastic changes to the breast epithelium and tumor formation. Cancer Res. 2012;72:2672–82.
3. Yarden Y, Pines G. The ERBB network: at last, cancer therapy meets systems biology. Nat Rev Cancer. 2012;12:553–63.
4. Slamon DJ, Leyland-Jones B, Shak S, Fuchs H, Paton V, Bajamonde A, et al. Use of chemotherapy plus a monoclonal antibody against HER2 for metastatic breast cancer that overexpresses HER2. N Engl J Med. 2001;344:783–92.
5. Mishra R, Patel H, Alanazi S, Yuan L, Garrett JT HER3 signaling and targeted therapy in cancer. Oncol Rev [Internet]. 2018 [cited

2020 Mar 10];12. https://www.ncbi.nlm.nih.gov/pmc/articles/PMC6047885/
6. Amin DN, Sergina N, Ahuja D, McMahon M, Blair JA, Wang D, et al. Resiliency and vulnerability in the HER2-HER3 tumorigenic driver. Sci Transl Med. 2010;2:16ra7.
7. Garrett JT, Olivares MG, Rinehart C, Granja-Ingram ND, Sánchez V, Chakrabarty A, et al. Transcriptional and posttranslational up-regulation of HER3 (ErbB3) compensates for inhibition of the HER2 tyrosine kinase. Proc Natl Acad Sci Usa 2011;108:5021–6.
8. Sergina NV, Rausch M, Wang D, Blair J, Hann B, Shokat KM, et al. Escape from HER-family tyrosine kinase inhibitor therapy by the kinase-inactive HER3. Nature 2007;445:437–41.
9. Chandarlapaty S, Sawai A, Scaltriti M, Rodrik-Outmezguine V, Grbovic-Huezo O, Serra V, et al. AKT inhibition relieves feedback suppression of receptor tyrosine kinase expression and activity. Cancer Cell. 2011;19:58–71.
10. Kodack DP, Askoxylakis V, Ferraro GB, Sheng Q, Badeaux M, Goel S, et al. The brain microenvironment mediates resistance in luminal breast cancer to PI3K inhibition through HER3 activation. Sci Transl Med. 2017 [cited 2020 Mar 10];9. https://www.ncbi.nlm.nih.gov/pmc/articles/PMC5917603/
11. Gijsen M, King P, Perera T, Parker PJ, Harris AL, Larijani B, et al. HER2 phosphorylation is maintained by a PKB negative feedback loop in response to anti-HER2 herceptin in breast cancer. PLoS Biol. 2010;8:e1000563.
12. Xia W, Petricoin EF, Zhao S, Liu L, Osada T, Cheng Q, et al. An heregulin-EGFR-HER3 autocrine signaling axis can mediate acquired lapatinib resistance in HER2+ breast cancer models. Breast Cancer Res BCR. 2013;15:R85.
13. Kang JC, Poovassery JS, Bansal P, You S, Manjarres IM, Ober RJ, et al. Engineering multivalent antibodies to target heregulin-induced HER3 signaling in breast cancer cells. mAbs. 2014;6:340–53.
14. Willnow TE, Carlo A-S, Rohe M, Schmidt V. SORLA/SORL1, a neuronal sorting receptor implicated in Alzheimer's disease. Rev Neurosci. 2010;21:315–29.
15. Willnow TE, Petersen CM, Nykjaer A. VPS10P-domain receptors - regulators of neuronal viability and function. Nat Rev Neurosci. 2008;9:899–909.
16. Andersen OM, Reiche J, Schmidt V, Gotthardt M, Spoelgen R, Behlke J, et al. Neuronal sorting protein-related receptor sorLA/LR11 regulates processing of the amyloid precursor protein. Proc Natl Acad Sci USA. 2005;102:13461–6.
17. Schmidt V, Schulz N, Yan X, Schürmann A, Kempa S, Kern M, et al. SORLA facilitates insulin receptor signaling in adipocytes and exacerbates obesity. J Clin Invest. 2016;126:2706–20.
18. Fjorback AW, Seaman M, Gustafsen C, Mehmedbasic A, Gokool S, Wu C, et al. Retromer binds the FANSHY sorting motif in SorLA to regulate amyloid precursor protein sorting and processing. J Neurosci J Soc Neurosci. 2012;32:1467–80.
19. Jacobsen L, Madsen P, Nielsen MS, Geraerts WPM, Gliemann J, Smit AB, et al. The sorLA cytoplasmic domain interacts with GGA1 and -2 and defines minimum requirements for GGA binding. FEBS Lett. 2002;511:155–8.
20. Al-Akhrass H, Naves T, Vincent F, Magnaudeix A, Durand K, Bertin F, et al. Sortilin limits EGFR signaling by promoting its internalization in lung cancer. Nat Commun. 2017;8:1–15.
21. Caldieri G, Malabarba MG, Di Fiore PP, Sigismund S. EGFR trafficking in physiology and cancer. Prog Mol Subcell Biol. 2018;57:235–72.
22. Bertelsen V, Stang E. The mysterious ways of ErbB2/HER2 trafficking. Membranes. 2014;4:424–46.
23. Pietilä M, Sahgal P, Peuhu E, Jäntti NZ, Paatero I, Närvä E, et al. SORLA regulates endosomal trafficking and oncogenic fitness of HER2. Nat Commun. 2019;10:2340.
24. Barretina J, Caponigro G, Stransky N, Venkatesan K, Margolin AA, Kim S, et al. The Cancer Cell Line Encyclopedia enables predictive modeling of anticancer drug sensitivity. Nature. 2012;483:603–7.
25. Cerami E, Gao J, Dogrusoz U, Gross BE, Sumer SO, Aksoy BA, et al. The cBio cancer genomics portal: an open platform for exploring multidimensional cancer genomics data. Cancer Disco. 2012;2:401–4.
26. Gao J, Aksoy BA, Dogrusoz U, Dresdner G, Gross B, Sumer SO, et al. Integrative analysis of complex cancer genomics and clinical profiles using the cBioPortal. Sci Signal. 2013;6:pl1.
27. Pereira B, Chin S-F, Rueda OM, Vollan H-KM, Provenzano E, Bardwell HA, et al. The somatic mutation profiles of 2,433 breast cancers refines their genomic and transcriptomic landscapes. Nat Commun. 2016;7:11479.
28. Mei L, Nave K-A. Neuregulin-ERBB signaling in nervous system development and neuropsychiatric diseases. Neuron 2014;83 (Jul):27–49.
29. Zhang S, Huang W-C, Zhang L, Zhang C, Lowery FJ, Ding Z, et al. Src family kinases as novel therapeutic targets to treat breast cancer brain metastases. Cancer Res. 2013;73:5764–74.
30. Nusinow DP, Szpyt J, Ghandi M, Rose CM, McDonald ER, Kalocsay M, et al. Quantitative proteomics of the cancer cell line encyclopedia. Cell. 2020;180:387–402.e16.
31. Hu C-D, Chinenov Y, Kerppola TK. Visualization of interactions among bZIP and Rel family proteins in living cells using bimolecular fluorescence complementation. Mol Cell. 2002;9:789–98.
32. Croucher DR, Iconomou M, Hastings JF, Kennedy SP, Han JZR, Shearer RF, et al. Bimolecular complementation affinity purification (BiCAP) reveals dimer-specific protein interactions for ERBB2 dimers. Sci Signal. 2016;9:ra69.
33. Schuck P. Use of surface plasmon resonance to probe the equilibrium and dynamic aspects of interactions between biological macromolecules. Annu Rev Biophys Biomol Struct. 1997;26:541–66.
34. Maxfield FR, McGraw TE. Endocytic recycling. Nat Rev Mol Cell Biol. 2004;5:121–32.
35. Wang C, Wang Y, Li Y, Bodemann B, Zhao T, Ma X, et al. A nanobuffer reporter library for fine-scale imaging and perturbation of endocytic organelles. Nat Commun. 2015;6:8524.
36. Mehmedbasic A, Christensen SK, Nilsson J, Rüetschi U, Gustafsen C, Poulsen ASA, et al. SorLA complement-type repeat domains protect the amyloid precursor protein against processing. J Biol Chem. 2015;290:3359–76.
37. Navaroli DM, Bellvé KD, Standley C, Lifshitz LM, Cardia J, Lambright D, et al. Rabenosyn-5 defines the fate of the transferrin receptor following clathrin-mediated endocytosis. Proc Natl Acad Sci USA. 2012;109:E471–480.
38. Small SA, Petsko GA. Retromer in Alzheimer disease, Parkinson disease and other neurological disorders. Nat Rev Neurosci. 2015;16:126–32.
39. Grant BD, Donaldson JG. Pathways and mechanisms of endocytic recycling. Nat Rev Mol Cell Biol. 2009;10:597–608.
40. Ding Y, Gong C, Huang D, Chen R, Sui P, Lin KH, et al. Synthetic lethality between HER2 and transaldolase in intrinsically resistant HER2-positive breast cancers. Nat Commun [Internet]. 2018 Oct [cited 2020 Mar 23];9. https://www.ncbi.nlm.nih.gov/pmc/articles/PMC6189078/
41. Baselga J, Im S-A, Iwata H, Cortés J, Laurentiis MD, Jiang Z, et al. Buparlisib plus fulvestrant versus placebo plus fulvestrant in postmenopausal, hormone receptor-positive, HER2-negative, advanced breast cancer (BELLE-2): a randomised, double-blind, placebo-controlled, phase 3 trial. Lancet Oncol. 2017;18:904–16.
42. Liu J, Duan Z, Guo W, Zeng L, Wu Y, Chen Y, et al. Targeting the BRD4/FOXO3a/CDK6 axis sensitizes AKT inhibition in

luminal breast cancer. Nat Commun. 2018 [cited 2020 Mar 23];9. https://www.ncbi.nlm.nih.gov/pmc/articles/PMC6281582/
43. Boulbes DR, Chauhan GB, Jin Q, Bartholomeusz C, Esteva FJ. CD44 expression contributes to trastuzumab resistance in HER2-positive breast cancer cells. Breast Cancer Res Treat. 2015;151:501–13.
44. Fazio M, Ablain J, Chuan Y, Langenau DM, Zon LI. Zebrafish patient avatars in cancer biology and precision cancer therapy. Nat Rev Cancer. 2020;20:263–73.
45. Falls DL. Neuregulins: functions, forms, and signaling strategies. Exp Cell Res. 2003;284:14–30.
46. Hutcheson IR, Goddard L, Barrow D, McClelland RA, Francies HE, Knowlden JM, et al. Fulvestrant-induced expression of ErbB3 and ErbB4 receptors sensitizes oestrogen receptor-positive breast cancer cells to heregulin β1. Breast Cancer Res BCR. 2011;13:R29.
47. Tomas A, Futter CE, Eden ER. EGF receptor trafficking: consequences for signaling and cancer. Trends Cell Biol. 2014;24:26–34.
48. Tubbesing K, Ward J, Abini-Agbomson R, Malhotra A, Rudkouskaya A, Warren J, et al. Complex Rab4-Mediated Regulation of Endosomal Size and EGFR Activation. Mol Cancer Res. 2020 [cited 2020 Mar 30];(19–0052). https://mcr.aacrjournals.org/content/early/2020/03/03/1541-7786.MCR-19-0052
49. Parachoniak CA, Luo Y, Abella JV, Keen JH, Park M. GGA3 functions as a switch to promote met receptor recycling, essential for sustained ERK and cell migration. Dev Cell. 2011;20:751–63.
50. Roselli S, Pundavela J, Demont Y, Faulkner S, Keene S, Attia J, et al. Sortilin is associated with breast cancer aggressiveness and contributes to tumor cell adhesion and invasion. Oncotarget 2015;6:10473–86.
51. Rhost S, Hughes É, Harrison H, Rafnsdottir S, Jacobsson H, Gregersson P, et al. Sortilin inhibition limits secretion-induced progranulin-dependent breast cancer progression and cancer stem cell expansion. Breast Cancer Res BCR. 2018;20:137.
52. Kodack DP, Chung E, Yamashita H, Incio J, Duyverman AMMJ, Song Y, et al. Combined targeting of HER2 and VEGFR2 for effective treatment of HER2-amplified breast cancer brain metastases. Proc Natl Acad Sci USA. 2012;109:E3119–3127.
53. Kodack DP, Askoxylakis V, Ferraro GB, Fukumura D, Jain RK. Emerging strategies for treating brain metastases from breast cancer. Cancer Cell. 2015;27:163–75.
54. Olson EM, Abdel-Rasoul M, Maly J, Wu CS, Lin NU, Shapiro CL.Incidence and risk of central nervous system metastases as site of first recurrence in patients with HER2-positive breast cancer treated with adjuvant trastuzumab.Ann Oncol. 2013;24:1526–33.
55. Sato T, Sato F, Kamezaki A, Sakaguchi K, Tanigome R, Kawakami K, et al. Neuregulin 1 type II-ErbB signaling promotes cell divisions generating neurons from neural progenitor cells in the developing zebrafish brain. PloS One. 2015;10:e0127360.
56. Research C for DE and. FDA approves neratinib for metastatic HER2-positive breast cancer. FDA. 2020 [cited 2020 Mar 30]; http://www.fda.gov/drugs/resources-information-approved-drugs/fda-approves-neratinib-metastatic-her2-positive-breast-cancer
57. Zhang Y, Zhang J, Liu C, Du S, Feng L, Luan X, et al. Neratinib induces ErbB2 ubiquitylation and endocytic degradation via HSP90 dissociation in breast cancer cells. Cancer Lett. 2016;382:176–85.
58. Schneider CA, Rasband WS, Eliceiri KW. NIH Image to ImageJ: 25 years of image analysis. Nat Methods. 2012;9:671–5.
59. Heid CA, Stevens J, Livak KJ, Williams PM. Real time quantitative PCR. Genome Res. 1996;6:986–94.
60. Fréal A, Rai D, Tas RP, Pan X, Katrukha EA, van de Willige D, et al. Feedback-driven assembly of the axon initial segment. Neuron 2019;104:305–21.e8.
61. Peuhu E, Virtakoivu R, Mai A, Wärri A, Ivaska J. Epithelial vimentin plays a functional role in mammary gland development. Dev Camb Engl. 2017;144:4103–13.
62. Johannessen CM, Boehm JS, Kim SY, Thomas SR, Wardwell L, Johnson LA, et al. COT drives resistance to RAF inhibition through MAP kinase pathway reactivation. Nature 2010;468:968–72.
63. Graham FL, van der Eb AJ. A new technique for the assay of infectivity of human adenovirus 5 DNA. Virology 1973;52:456–67.
64. White RM, Sessa A, Burke C, Bowman T, LeBlanc J, Ceol C, et al. Transparent adult zebrafish as a tool for in vivo transplantation analysis. Cell Stem Cell. 2008;2:183–9.
65. Paatero I, Alve S, Gramolelli S, Ivaska J, Ojala P Zebrafish embryo xenograft and metastasis assay. BIO-Protoc. 2018 [cited 2020 Mar 25];8. https://bio-protocol.org/e3027